Available online at www.sciencedirect.com
SCIENCE DIRECT®
International Journal of Heat and Mass Transfer 49 (2006) 3984–3996
International Journal of HEAT and MASS TRANSFER
www.elsevier.com/locate/ijhmt

Effect of optical properties on oscillatory hydromagnetic double-diffusive convection within semitransparent fluid

Mohamed Naceur Borjini [a], Habib Ben Aissia [b], Kamel Halouani [c], Belkacem Zeghmati [d,*]

[a] Département de Physique, Faculté des Sciences 5019 Monastir, Tunisia
[b] Ecole Nationale d'Ingénieurs, 5012 Monastir, Tunisia
[c] METS – ENIS – IPEIS – Route Menzel Chaker B.P: 805, 3000 Sfax, Tunisia
[d] MEPS-GME, Université de Perpignan Via Domitia, 52 Avenue Paul Alduy, 68660 Perpignan Cedex, France

Received 2 June 2005; received in revised form 24 February 2006
Available online 19 June 2006

Abstract

The effect of radiative heat transfer on the hydromagnetic double-diffusive convection in two-dimensional rectangular enclosure is studied numerically for fixed Prandtl, Rayleigh, and Lewis numbers, $Pr = 13.6$, $Ra = 10^5$, $Le = 2$. Uniform temperatures and concentrations are imposed along the vertical walls while the horizontal walls are assumed to be adiabatic and impermeable to mass transfer. The influences of the optical thickness and scattering albedo of the semitransparent fluid on heat and mass transfer with and without magnetic damping are depicted. When progressively varying the optical thickness, multiple solutions are obtained which are steady or oscillatory accordingly to the initial conditions. the mechanisms of the transitions between steady compositionally dominated flow and unsteady thermally dominated flow are analyzed.

Keywords: Hydromagnetic double-diffusive convection; Internal radiation; Radiative properties; Thermosolutal instability

1. Introduction

The double-diffusive convection, which takes place when compositionally driven buoyant convection and thermally driven buoyant convection occur simultaneously, arises in a very wide range of fields such as oceanography, astrophysics, chemical vapour transport process, drying process, crystal growth process, etc. This convection was widely experimentally and numerically studied for varied several non-dimensional parameters namely the Lewis and Prandtl numbers, the buoyancy ratio and for either aiding or opposing heat and mass gradients. Reviews on this subject can be found in the publications of Nishumira et al. [1], Ostrach [2], Viskanta et al. [3], Béghein et al. [4], Zhou and Zebib [5], Chamkha and Al-Naser [6], Costa [7,8] and Papanicalaou and Belessiotis [9]. It has been found that, for a buoyancy ratio close to the unity, an oscillatory flow caused by the interaction between thermal and compositional recirculations occurs. Nishumira et al. [1] carried out a careful depiction of the mechanism of this oscillatory flow. For the crystal growth process, the double-diffusive convection is induced because of the non-uniform distribution of impurities [10] and the quality of the growing crystal is severely affected by the melt convection and any oscillations are disadvantageous.

The request of an external magnetic field to control fluid flow and heat transfer in electrically conducting fluids has long been recognized in many applications such as crystal growth. Numerous studies on magnetoconvection were presented in the last few years especially for lower values of Prandtl number. Detailed bibliography can be found in Grandet et al. [11], Mößner and Müller [12] and Chamkha and Al-Naser [6]. Lately Aleksandrova and Molokov

* Corresponding author.
E-mail addresses: naceur.borjini@fsm.rnu.tn (M.N. Borjini), Habib.benaissia@enim.rnu.tn (H.B. Aissia), Kamel.Halouani@ipeis.rnu.tn (K. Halouani), Zeghmati@univ-perp.fr (B. Zeghmati).

0017-9310/$ - see front matter © 2006 Elsevier Ltd. All rights reserved.
doi:10.1016/j.ijheatmasstransfer.2006.03.041

Nomenclature

B_0	magnetic induction
C	dimensionless species concentration, $C = (C' - C'_l)/(C'_h - C'_l)$
C_h	high species concentration
C_l	low species concentration
D	species diffusivity
g	acceleration of gravity
H	enclosure height
Ha	Hartmann number, $Ha = B_0 W\sqrt{\sigma_e/\mu}$
I	dimensionless radiant intensity, $I = I'/(n^2\sigma(T'_c)^4/\pi)$
I^0	dimensionless black body intensity, $I^0 = I^{0\prime}/(n^2\sigma(T'_c)^4/\pi)$
L	total number of discrete solid angles
L_+	total number of discrete solid angles oriented to a given boundary
Le	Lewis number, $Le = \alpha/D$
N	dimensionless quantity, $N_i^l = \frac{1}{\Delta\Omega^l}\int_{\Delta\Omega^l}\mathbf{\Omega}\mathbf{n}_i\,d\Omega$
N	buoyancy ratio, $N = \beta_C(C'_h - C'_l)/\beta_T(T'_h - T'_c)$
n	refractive index
$\mathbf{n}$	unit vector normal to the control volume surface
Pr	Prandtl number, $Pr = \nu/\alpha$
Qc	dimensionless conductive heat flux averaged on isothermal walls
Qr	dimensionless radiative heat flux averaged on isothermal walls
Ra	Rayleigh number, $Ra = \beta_T g(T'_h - T'_c)W^3/(\nu\alpha)$
Rc	radiation conduction parameter, $Rc = n^2 W T_c^3\sigma/\lambda$
s	distance in the direction $\mathbf{\Omega}$ of the intensity
Sh	averaged Sherwood number defined in Eq. (14)
T	dimensionless temperature, $T = (T' - T'_c)/(T'_h - T'_c)$
t	dimensionless time, $t = \alpha t'/W^2$
T'_h	hot wall temperature
T'_c	cold wall temperature
u	dimensionless horizontal velocity, $u = u'W/\alpha$
v	dimensionless vertical velocity, $v = v'W/\alpha$
W	enclosure width
x, y	dimensionless Cartesian coordinates, $x = x'/W$, $y = y'/W$

Greek symbols

α	thermal diffusivity
β_T	coefficient of thermal expansion
β_C	coefficient of compositional expansion
β_r	extinction coefficient, $\beta_r = \sigma_r + \kappa$
ΔA	area of a control volume face
Δv	control volume
$\Delta\Omega$	control solid angle
ε_v	emissivity of vertical walls
ε_h	emissivity of horizontal walls
ϕ	temperature ratio, $\phi = T'_h/T'_c - 1$
κ	absorption coefficient
λ	thermal conductivity
μ	dynamic viscosity
ν	kinematic viscosity
σ	Stefan–Boltzmann constant
σ_e	electrical conductivity
σ_r	scattering coefficient
τ	optical width, $\tau = \beta_r W$
ω	dimensionless vorticity, $\omega = \omega' W^2/\alpha$
ω_0	scattering albedo, $\omega_0 = \sigma_r/\beta_r$
$\mathbf{\Omega}$	unit vector in the direction of the intensity
ψ	dimensionless stream function, $\psi = \psi'/\alpha$

Subscripts

e, w, n, s	faces of control volume centred in P
E, W, N, S	nodes around the nodal point P
P	nodal points

Superscripts

$'$	real variables
l, l'	discrete angular directions

[13] presented a three-dimensional study of buoyant convection in a rectangular cavity in presence of a strong magnetic field and Kenjeres and Hanjalic [14] considered magnetoconvection in fully turbulent regime and numerically studied, in addition to the magnetic damping, the laminarization effect of the external magnetic field. It has been found [12] that for a horizontal temperature gradient, a magnetic field perpendicular to the heated wall is most effective in damping the natural convection.

In crystal growth process of optical materials such as yttrium aluminum garnet (YAG), gadolinium gallium garnet (GGG) and lithium niobate (LN), the internal radiative heat transfer has a strong influence on the temperature distribution which affects the growing crystal quality. Taking the radiative heat transfer within both the crystal and the melt into account, Tsukada et al. [15] accomplished a global analysis of heat transfer for the crystal growth of an oxide ($LiNbO_3$). The authors used the differential approximation P1 to model radiative heat transfer in grey-emitting media. Their results show a noteworthy impact of optical properties of the crystal and the melt on flow and temperature fields. Especially, the melt–crystal interface shape becomes more convex toward the melt as the optical absorption coefficients of both the crystal and the melt decrease. Considering similar crystal, Kobayashi et al. [16,17] adopted the S4 discrete ordinates method to model

radiative heat transfer in absorbing–emitting grey melt. They studied the effect of the absorption coefficient on transition between steady flow and oscillatory flow. This oscillatory behaviour is due to the competition between the natural convection and the forced convection caused by the crystal rotation. Using the differential approximation P1, Kobayashi et al. [18] analyzed the effect of internal radiation in both the crystal and the melt on the inversion of their interface. The authors proved that the critical Reynolds number at which the interface inversion occurs depends on the optical thickness of the melt and the crystal. By adopting the S4 discrete ordinates method in three-dimensional non-axisymmetric geometry, Jing et al. [19] analyzed the effect of internal radiative heat transfer on spoke pattern in $LiNbO_3$ melt. For radiatively participating melt, the spoke pattern disappeared and the flow became steady and axisymmetric. Lan et al. [20] used both the P1 and the Rosseland approximations to model internal radiation in Bridgman growth of YAG crystals. A detailed analysis of studies taking into account radiative heat transfer in modelling crystal growth was carried out by Brandon and Derby [21] and recently by Müller and Friedrich [22]. Jing et al. [23] performed a three-dimensional numerical simulation of spoke pattern in a $LiNbO_3$ oxide melt under a magnetic field but they neglected the internal radiative heat transfer. By studying double-diffusive convection during alloyed semiconductor crystal growth in strong axial and transverse magnetic fields, Farrel and Ma [24] mentioned that magnetic field must be strong enough to eliminate flow oscillations but which moderately damped the melt motion in order to achieve both lateral and axial compositional uniformity in the crystal.

Given that many oxide crystals are semitransparent and their absorption coefficients vary depending on the amount of dopant added [18], it is convincing to study the effect of the optical thickness on the convective flow. It has been found experimentally [19] for $LiTaO_3$ Czochralski growth, that in N_2 atmosphere, a steady spoke pattern is detected, and in the melt the temperature is oscillatory. Nevertheless if O_2 is introduced into the growth atmosphere, both the spoke pattern and the temperature oscillations withdraw. The experimenters assign this behaviour to the change of the optical properties of the melt [19]. Indeed, these experimental measures show that for the first situation the melt can be regarded as opaque while for the second case the melt is semitransparent. Accordingly, radiative heat transfer in the melt works as a stabilizer for Marongani instability and it affords, by changing the growth atmosphere, the aptitude to tailor the melt flow in order to improve the quality of the crystal.

In the present work, the effect of the optical properties of a radiatively participating fluid on oscillatory hydromagnetic double-diffusive convection in a rectangular enclosure is numerically studied. A parametric study of the optical thickness for different values of Hartmann number is developed. This allows us to study the stabilizing effect of the internal radiation on this thermosolutal instability for flows with or without magnetic damping. Results show a quantitative dependence of this effect on the applied external magnetic field for moderately damped flow while the highly damped flow is always steady. Then the effect of the scattering albedo on heat and mass transfer is rapidly discussed. To the best knowledge of the authors, no study concerning the influence of the optical properties on oscillatory hydromagnetic double-diffusive convection with radiative heat transfer has been published.

2. Mathematical formulation and numerical modelling

As represented in Fig. 1, the physical system consists of a rectangular enclosure with $H/W = 2$ as aspect ratio and with uniform imposed temperatures and concentrations along the left and right vertical walls. The horizontal walls are assumed to be adiabatic and impermeable to mass transfer. All enclosure walls are grey, diffuse, and have different emissivities. The electrically conducting rectangular melt is considered as a grey, emitting, absorbing, and isotropically scattering fluid. Initially, the medium is at a uniform temperature T'_c, and concentration C'_l while the temperature and concentration of the left vertical wall are abruptly changed to higher values T'_h and C'_h respectively while those on the right wall are maintained at T'_c and C'_l respectively. The flow in the system is supposed laminar with no-slip conditions at the walls, the physical properties are constant, and the Boussinesq approximation is valid. The viscous dissipation, Soret and Dufour effects, and induced magnetic field are neglected. As discussed by Garandet et al. [11], for two-dimensional study, the harmonic equation of the electric potential is valid in the melt as well as in the neighbouring solid media. Since there is always an electrically insulating boundary, the unique solution coincides with a vanishing electric field.

When scaling length, velocity, and time by W, α/W and W^2/α, and defining dimensionless temperature and concentration $T = (T' - T'_c)/(T'_h - T'_c)$ and $C = (C' - C'_l)/$

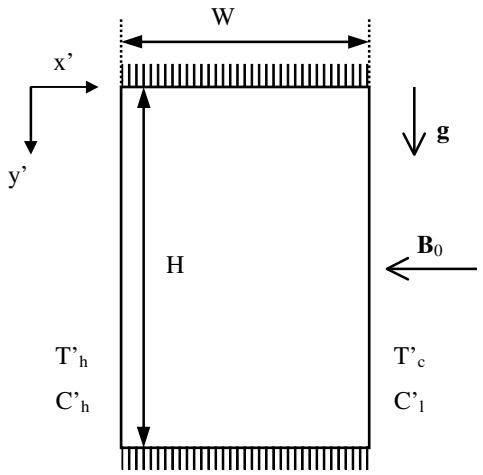

Fig. 1. Schematic description of the model.

$(C'_h - C'_l)$, the governing equations in dimensionless stream function-vorticity form are:

$$\frac{\partial^2\psi}{\partial x^2} + \frac{\partial^2\psi}{\partial y^2} = -\omega \tag{1}$$

$$\frac{\partial\omega}{\partial t} + \frac{\partial}{\partial x}\left(u\omega - Pr\frac{\partial\omega}{\partial x}\right) + \frac{\partial}{\partial y}\left(v\omega - Pr\frac{\partial\omega}{\partial y}\right) = PrRa\left[-\frac{\partial T}{\partial x} + N\frac{\partial C}{\partial x}\right] - Ha^2Pr\frac{\partial v}{\partial x} \tag{2}$$

$$\frac{\partial T}{\partial t} + \frac{\partial}{\partial x}\left(uT - \frac{\partial T}{\partial x}\right) + \frac{\partial}{\partial y}\left(vT - \frac{\partial T}{\partial y}\right) = \frac{\mathrm{Rc}(1-\omega_0)\tau}{\Phi\pi}\left[\int I\,\mathrm{d}\Omega - 4\pi(1+\Phi T)^4\right] \tag{3}$$

$$\frac{\partial C}{\partial t} + \frac{\partial}{\partial x}\left(uC - \frac{1}{Le}\frac{\partial C}{\partial x}\right) + \frac{\partial}{\partial y}\left(vC - \frac{1}{Le}\frac{\partial C}{\partial y}\right) = 0 \tag{4}$$

In the absence of any contrary indication, the associated initial and boundary conditions for the considered problem are:

For $t \leqslant 0$

$$\omega = \psi = \frac{\partial\psi}{\partial x} = \frac{\partial\psi}{\partial y} = T = C = 0 \text{ (everywhere)} \tag{5}$$

For $t > 0$

on the heated wall $(x = 0)$

$$\psi = \frac{\partial\psi}{\partial x} = 0, \quad T = C = 1 \tag{6}$$

on the cooled wall $(x = 1)$

$$\psi = \frac{\partial\psi}{\partial x} = T = C = 0 \tag{7}$$

on the adiabatic walls $(y = 0, 2)$

$$\psi = \frac{\partial\psi}{\partial y} = \frac{\partial T}{\partial y} = \frac{\partial C}{\partial y} = 0 \tag{8}$$

For a grey absorbing, emitting, and isotropically scattering medium, the radiative transfer equation can be written as [25].

$$\frac{\partial I(s,\mathbf{\Omega})}{\partial s} + \beta_r I(s,\mathbf{\Omega}) = \beta_r R \tag{9}$$

where

$$R = (1-\omega_0)I^0(s) + \frac{\omega_0}{4\pi}\int_{4\pi} \mathrm{I}(s,\mathbf{\Omega})d\mathbf{\Omega} \tag{10}$$

The finite volume method is utilised to discretize Eq. (9). The computational domain is divided into finite volumes and the intensity direction into finite number of solid angles. Then this equation is integrated over each control volume and control angle by using the step scheme. Further details on the finite volume method are in Chai et al. [26] and Borjini et al. [27].

Eqs. (1)–(4) are discretized using the control volume method [28]. The central-difference scheme for treating convective terms and the fully implicit procedure to discretize the temporal derivatives are retained. The grid is uniform in both directions with additional nodes on boundaries. The resulting non-linear algebraic equations are solved using the successive relaxation-iterating scheme [29]. The equation of radiative transfer is solved by repeatedly sweeping across grid until convergence without taking into account the optimal order in which the nodes should be visited. Additional details on the present numerical algorithm are in references [30,31]. The time step 10^{-4}, spatial mesh 31×41 and angular mesh 2×12 are retained. The solution is considered satisfactory when the following convergence criterion is verified for each time step:

$$\frac{\max|\psi^m - \psi^{m-1}|}{\max|\psi^m|} + \max|T^m - T^{m-1}| + \max|C^m - C^{m-1}| \leqslant 10^{-5} \tag{11}$$

where the superscript m assigns the iteration number.

The dimensionless conductive flux, radiative flux and Sherwood number are averaged and evaluated along the isothermal walls as follows:

average conductive flux (Nusselt number)

$$Q_c = \frac{1}{2}\int_0^2 -\frac{\partial T}{\partial x}\mathrm{d}y \tag{12}$$

average radiative flux:

$$Q_r = \frac{1}{2}\int_0^2 \sum_{l=1}^{L} N^l I^l \Delta\Omega^l \,\mathrm{d}y \tag{13}$$

average Sherwood number

$$Sh = \frac{1}{2}\int_0^2 -\frac{\partial C}{\partial x}\mathrm{d}y \tag{14}$$

The time-averaged values of these quantities are designated by $\overline{Q_c}$, $\overline{Q_r}$ and $\overline{Sh}$.

3. Validation

The present control volume method results are in good agreement with previous results. In fact, the temporal

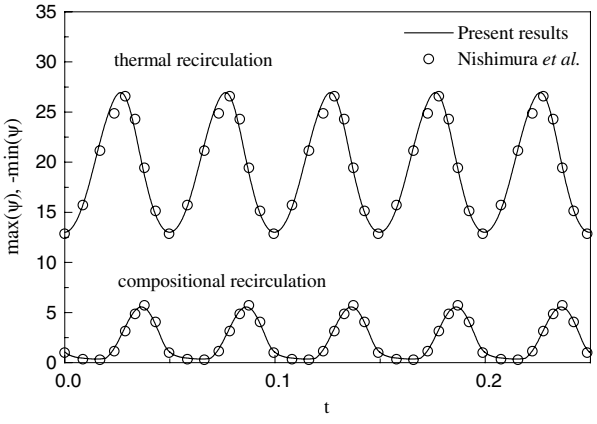

Fig. 2. Temporal behaviour of thermal and compositional recirculations for opaque fluid at $Pr = 1$, $Le = 2$, $Ra = 10^5$, $N = 1$ and $Ha = 0$.

Table 1
Comparison between the present results and other numerical methods for $N = 1$, $Le = 2$, $Ra = 10^5$, $Pr = 1$ and $Ha = 0$

	Finite-element (31×41) [1]	Spectral (40×80) [1]	Finite-difference (31×41) [6]	Control volume present results		
				(21×31)	(31×41)	(41×51)
Dimensionless period $\times 10^2$	4.97	4.94	5.091	5.075	4.998	4.992
$\mathrm{Max}\lvert\Psi_{max}\rvert$	26.7	26.8	27.8	27.67	26.94	26.91
$\mathrm{Min}\lvert\Psi_{max}\rvert$	12.9	12.7	13.7	13.33	13.02	12.97
$\mathrm{Max}\lvert\Psi_{min}\rvert$	5.76	5.52	5.85	5.68	5.56	5.55
$\mathrm{Min}\lvert\Psi_{min}\rvert$	0.351	0.333	0.333	0.323	0.356	0.349

behaviour of maximum and minimum stream function, shown in Fig. 2 for opaque fluid at $Ra = 10^5$, $Pr = 1$, $N = 1$, $Le = 2$ and $Ha = 0$, is in perfect accord with Nishumira et al. [1] results for both thermal and compositional recirculation. This is quantitatively approved in Table 1 showing comparison between the present method and three numerical methods for the dimensionless period of oscillation and stream function extremes. This table also justifies the use of 31×41 spatial meshes at least for $Ra \leqslant 10^5$.

In Fig. 3, comparisons between the present method and the finite-difference method results [7] in the presence of an external magnetic field are illustrated for the averaged Sherwood and Nusselt numbers. These results are in satisfactory agreement with a maximum relative difference about 5% for weak Hartmann numbers. Obviously, increasing Ha decreases both Nusselt and Sherwood numbers and the damping effect is available for both compositionally dominated ($N = 1.3$) and thermally dominated ($N = 0.8$) flows. Supplementary validation of the present combined convective–radiative model can be found in [30,31].

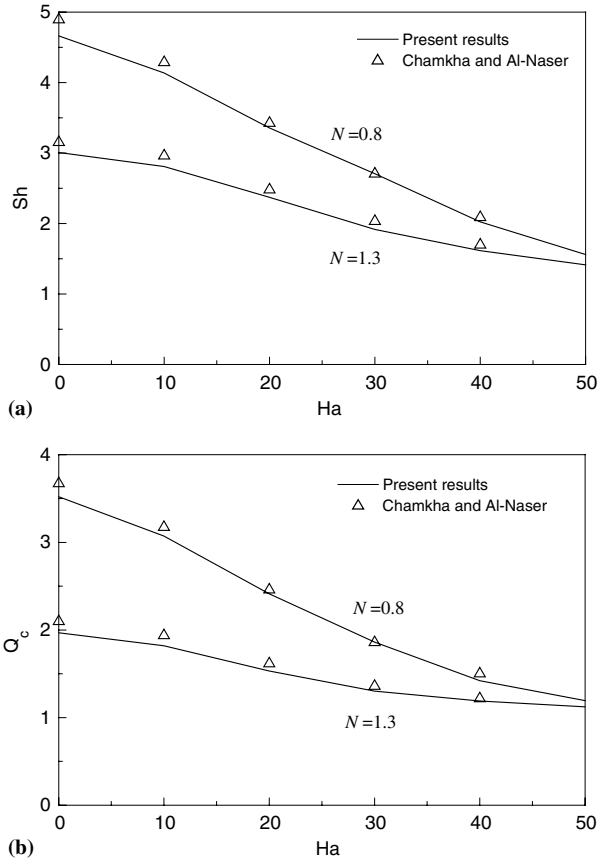

Fig. 3. Magnetic damping of mass transfer (a) and conductive heat transfer (b) for both compositionally dominated and thermally dominated flows and for opaque fluid at $Pr = 1$, $Le = 2$ and $Ra = 10^5$.

4. Results and discussion

4.1. Effect of optical thickness

A parametric study of the optical thickness for different values of Hartmann number is developed for $Le = 2$, $N = 1$, $Ra = 10^5$, $Pr = 13.6$, $\mathrm{Rc} = 1$ and $\phi = 0.1$. Computations are performed for perfectly reflecting adiabatic walls and black isothermal walls. For a buoyancy ratio near unity, interaction between thermal-buoyancy and compositional-buoyancy forces leads to an interesting oscillatory flow, which justified the affectation of N. The selected Prandtl number value corresponds to the radiatively participating $LiNbO_3$ melt [17] and the affectation of the Lewis number is arbitrary. In fact, there is a lack of knowledge regarding physicochemical properties of oxide melts, such as the electrical conductivity and dissociation equilibrium [32]. By using the motionless state (Eqs. (5)–(8)) as initial condition, an oscillatory thermally dominated flow is obtained for $\tau = 10^{-2}$ and 10^2 and a steady compositionally dominated flow is established for $\tau = 1$. This is true for $Ha = 0$ and 10 while for $Ha = 40$, the flow is always steady. These solutions are used as initial conditions then the decimal logarithm of the optical thickness is gradually increased and decreased by 1/10 and subsequently a new initial solution is obtained. Following this demarche, τ is varied in the interval $[10^{-2}, 10^2]$ for three different Hartmann numbers. In Figs. 7–9, 12 and 14, the levels for stream function contours are given by: $|\psi_j| = (\max|\psi| \cdot j)/(J + 1)$. J is the total number of contours for each cell and j appoints the number of the contour counted from the exterior of each cell. For temperature and concentration, levels are uniformly incremented from 0 to 1. The flow is called compositionally dominated if the cell working directly between the active walls is a trigonometric-rotating recirculation (sign +) and reversely for the thermally dominated flow.

4.1.1. Flow without magnetic damping (Ha = 0)

Fig. 4 represents the variations of the maximum of the stream function with the optical thickness in the absence of the external magnetic field. If the initial condition is the steady compositionally dominated flow, the system "bifurcates" among steady and oscillatory states at some critical values of the optical thickness. Precisely, the system shifts from the steady compositionally dominated flow to an oscillatory thermally dominated flow at $\tau \approx 0.16$ ($\log\tau = -0.8$) and $\tau \approx 6.3$ ($\log\tau = 0.8$). If the initial state is the oscillatory thermally dominated flow, the solution is always unsteady independently of the optical thickness. However the amplitudes of oscillations are more important for optical thickness near unity. Similar coexistence of oscillatory and steady flows is found by Nishimura et al. [1]. However, Sezai and Mohamad [33] indicate that the double-diffusive flow in enclosures with opposing buoyancy forces is strictly three-dimensional for a certain range of parameters.

The temporal behaviour of the averaged Sherwood number, conductive and radiative fluxes on the hot wall, represented in Fig. 5, shows different oscillatory flows for three values of τ. The oscillations are complex for $\tau = 10^2$ and 10^{-2} but the absence of large broad band in the corresponding spectra (not shown here) attests that the flow is not fully chaotic. Qualitatively similar results are obtained on the cold wall. These oscillations are relatively weak for radiative fluxes, their frequency is almost insensitive to τ variations and their profiles are sensibly sinusoidal for optical thickness near unity. The effect of the optical thickness on the time-averaged values of these quantities is illustrated in Fig. 6. When τ increases, $\overline{Q_r}$ decreases while $\overline{Q_c}$ and $\overline{Sh}$ present a minimum for optical width near unity. This is restricted to oscillatory solutions and for the steady flow $\overline{Q_c}$ and $\overline{Sh}$ increase with τ but still lower than oscillatory levels and two stepped transitions of $\overline{Sh}$ and $\overline{Q_c}$ are observed for $\tau \approx 0.16$ and $\tau \approx 6.3$. Quantitatively and for oscillatory solutions, $\overline{Q_r}$ decreases by about 90% when τ changes from 10^{-2} to 10^2 while $\overline{Q_c}$ and $\overline{Sh}$ rise by about 15% and 20% respectively when τ varies between 1 and 10^2. Weaker rates are registered between 1 and 10^{-2}. For steady flow, the maximum relative upsurge of $\overline{Q_c}$ and $\overline{Sh}$ are about 30% and 20% respectively. In another hand and during the transitions, $\overline{Sh}$ rises by about 30% and

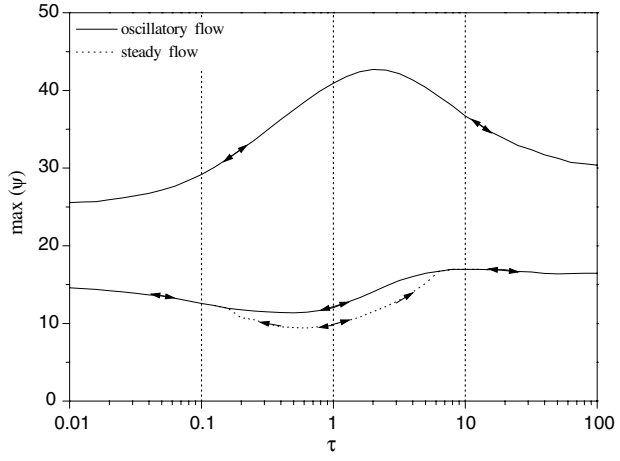

Fig. 4. Effect of the optical thickness on maximum stream function for $Pr = 13.6$, $Le = 2$, $Ra = 10^5$, $N = 1$, Rc = 1 and $Ha = 0$.

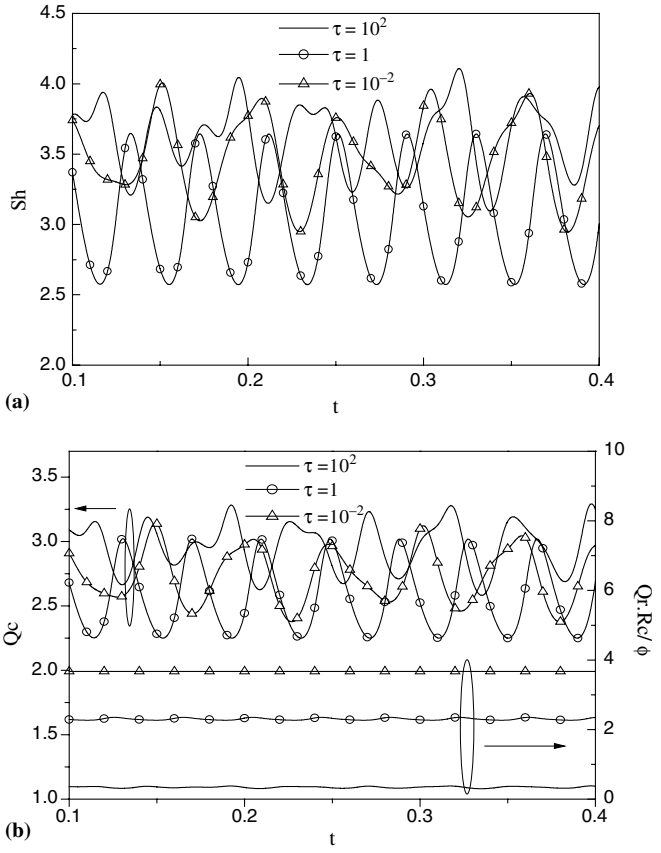

Fig. 5. Effect of the optical thickness on the temporal behaviour of Sherwood number (a) and conductive and radiative fluxes (b) for $Pr = 13.6$, $Le = 2$, $Ra = 10^5$, $N = 1$, Rc = 1 and $Ha = 0$.

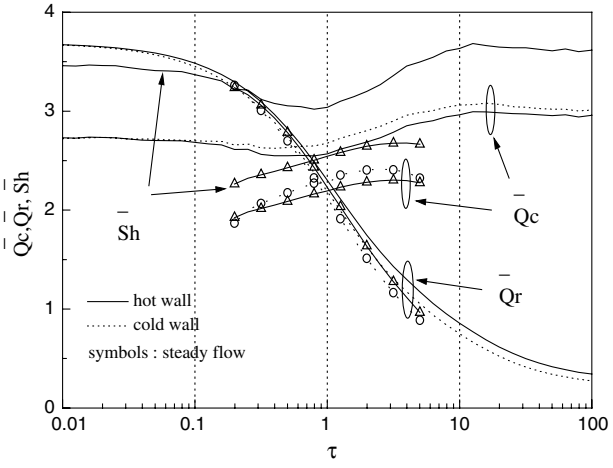

Fig. 6. Effect of the optical thickness on the time-averaged Sherwood number and conductive and radiative fluxes for $Pr = 13.6$, $Le = 2$, $Ra = 10^5$, $N = 1$, Rc = 1 and $Ha = 0$.

45% for right and left transitions on Fig. 6 respectively. The corresponding rates for $\overline{Q_c}$ are about 30% and 40%.

Fig. 7 shows that, the oscillatory flow is thermally dominated with two counter clockwise-rotating compositional recirculations (plus sign) at the top left and the bottom right corners and a large clockwise-rotating thermal recirculation (minus sign) in the core region and working directly between the isothermal walls. This flow structure is a consequence of the fact that, in the core of the cavity, the temperature gradient is larger than the concentration one [34]. The homogenization effect of the radiative heat transfer is more important for $\tau = 1$ and the core is heated which diminishes the temperature gradients near the vertical walls and consequently the related conductive fluxes. This gives good reason for the existence of the minimum of $\overline{Q_c}$ observed in Fig. 6. In another hand, the compositional recirculations are more developed for optically thick or thin media for which iso-concentration lines are more dense near the isothermal walls than in the case with $\tau = 1$. This endorses the minimum of mass transfer observed in Fig. 6. As shown in Fig. 8, the periodic behaviour for $\tau = 1$ consists on synchronized variations in the intensity and size of the corner cells with almost 1/4 period delay with the thermal cell which is the same delay obtained by Nishimura et al. [1] for $Pr = 1$ (see Fig. 2). Similar scenarios are observed for $\tau = 10^{\pm 2}$.

Fig. 9 shows that the steady flow is compositionally dominated with two clockwise-rotating important thermal recirculations at the top right and the bottom left corners and a counter clockwise-rotating compositional recirculation in the core region and working directly between the thermally active walls. This flow structure is a consequence of the fact that, in the core of the cavity, the concentration gradient is larger than the temperature gradient. As shown in Fig. 9, this compositionally dominated flow is transformed to a thermally dominated flow at $\tau \approx 0.16$ and 6.3 ($\log\tau = \pm 0.8$) via a coalescence of the two thermal cells. In fact, when $|\log\tau|$ rises, the left bottom recirculation expands and breaks up the compositional recirculation. The new thermally dominated oscillatory flow consists of a large right bottom compositional cell and a very weak left top recirculation (not represented). When $|\log\tau|$ increases again the flow coincides with that obtained when using oscillatory solutions as initial conditions. So, the mechanism of the two transitions is the same but isotherms and iso-concentrations are globally denser near vertical walls for $\tau \approx 6.3$ than for $\tau \approx 0.16$ which explains the profiles of $\overline{Q_c}$ and $\overline{Sh}$ in Fig. 6.

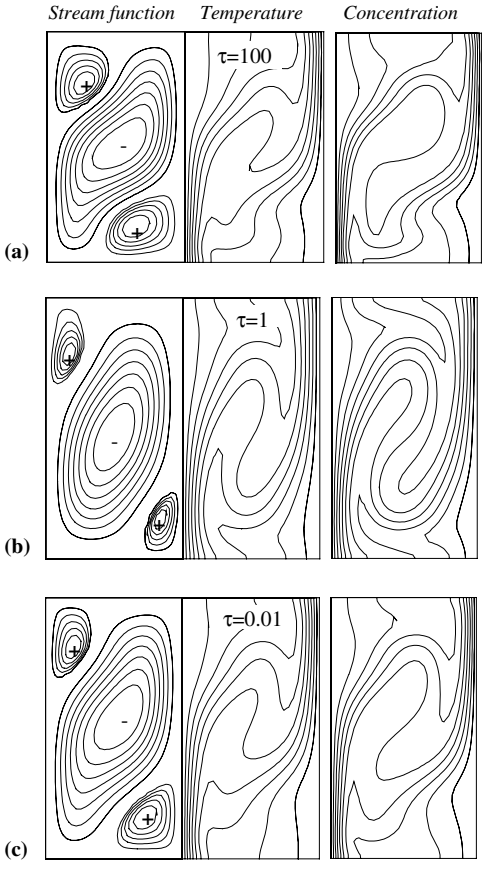

Fig. 7. Optical thickness influence on snapshots of oscillatory fields at $t = 0.2$. Computations are with oscillatory initial conditions and for $Pr = 13.6$, $Le = 2$, $Ra = 10^5$, $N = 1$, $\mathrm{Rc} = 1$ and $Ha = 0$. (−) clockwise-rotating flow, (+) counter clockwise-rotating flow. (a) $\max(\psi) = 23.8$, $\min(\psi) = -2.98$ (top cell), -4.11 (bottom cell); (b) $\max(\psi) = 39.9$, $\min(\psi) = -1.03$ (top cell), -0.73 (bottom cell); (c) $\max(\psi) = 23.85$, $\min(\psi) = -1.09$ (top cell), -1.39 (bottom cell).

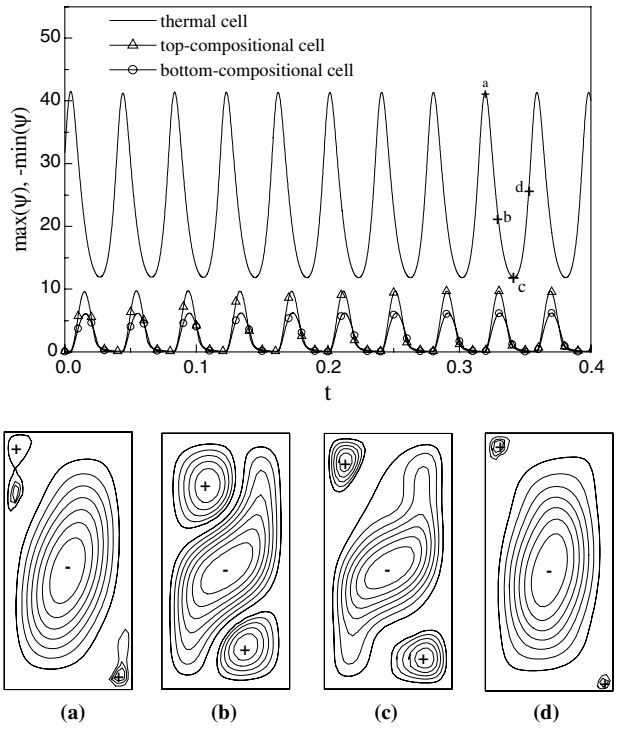

Fig. 8. Time behaviour and spatial structure of the flow during one period in absence of magnetic field and for $Pr = 13.6$, $Le = 2$, $Ra = 10^5$, $N = 1$, $\mathrm{Rc} = 1$ and $\tau = 1$.

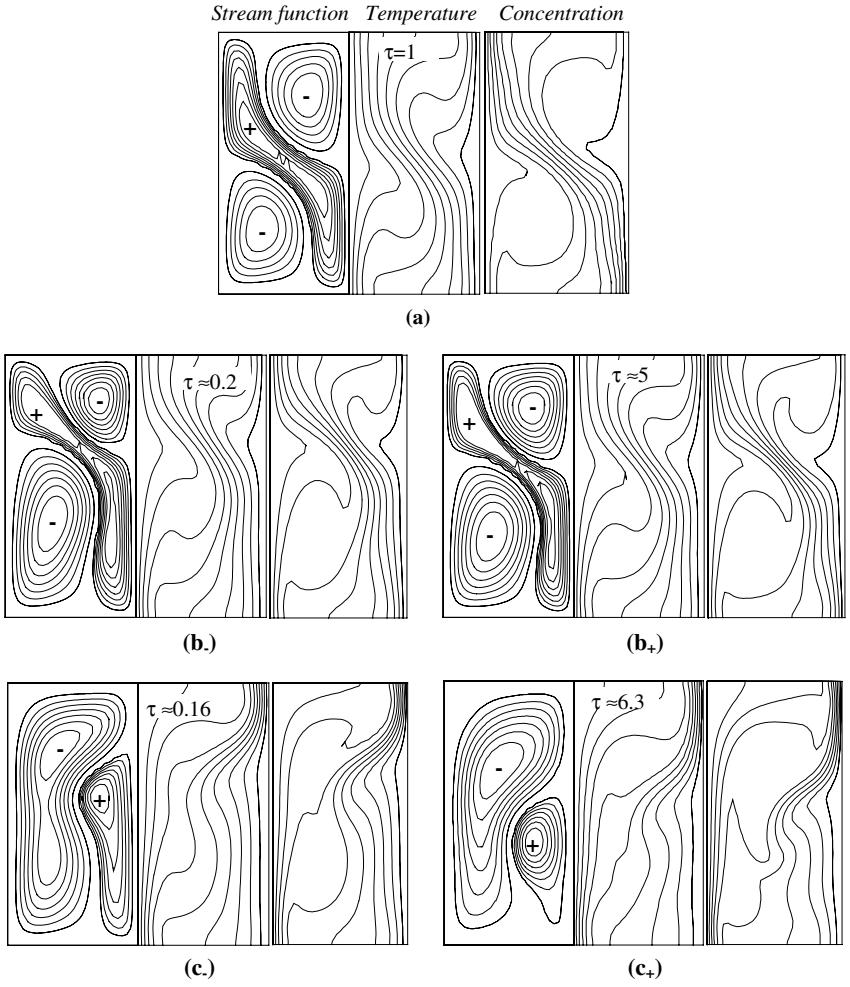

Fig. 9. Optical thickness influence on steady fields. Computations are with steady initial conditions and for $Pr = 13.6$, $Le = 2$, $Ra = 10^5$, $N = 1$, $\mathrm{Rc} = 1$ and $Ha = 0$. (a) $\min(\psi) = -2.8$, $\max(\psi) = 9.2$ (top cell), 9.8 (bottom cell) ; (b_+) $\min(\psi) = -2.33$, $\max(\psi) = 9.64$ (top cell), 14.93 (bottom cell); (b_-) $\min(\psi) = -1.88$, $\max(\psi) = 5.52$ (top cell), 11.3 (bottom cell); (c_+) $\max(\psi) = 24.1$, $\min(\psi) = -5.9$; (c_-) $\max(\psi) = 13.08$, $\min(\psi) = -2.25$.

4.1.2. Moderately damped flow ($Ha = 10$)

The same computations than the previous case are reproduced here with $Ha = 10$. Results using steady compositionally dominated and oscillatory thermally dominated initial conditions are very close and transitions from steady flow to unsteady flow (and reversely) are observed (Fig. 10). Like the non-damped case, the oscillatory flow is thermally dominated however, for intermediate values of τ, there is no oscillation for moderately damped flow. For optically thick media, the amplitudes of oscillations are very small and consequently, the stabilizing effect of the external magnetic field is most effective for strongly attenuating media. The transient behaviour of $\max(\psi)$ is represented in Fig. 11a for $\log\tau = 0.5$–0.8, and in Fig. 11b for $\log\tau = -0.9$ and -1. When $\log\tau$ changes from -1 to -0.9, the oscillatory flow transforms to a steady one. In fact, the bottom compositional cell expands, the top compositional recirculation disappears, and the flow is compositionally dominated near the cold wall and thermally dominated near the hot wall (Fig. 12b). This is confirmed by the corresponding isotherms and iso-concentrations showing relatively high horizontal gradients near the hot and the cold walls respectively. This structure is no longer retained and the compositional cell is repositioned in order to work directly between

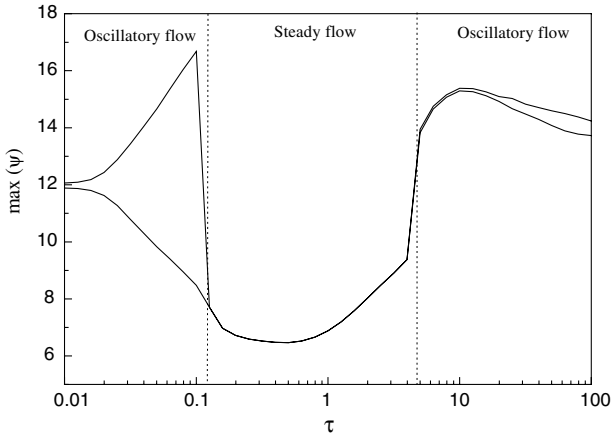

Fig. 10. Effect of the optical thickness on maximum stream function for $Pr = 13.6$, $Le = 2$, $Ra = 10^5$, $N = 1$, $\mathrm{Rc} = 1$ and $Ha = 10$.

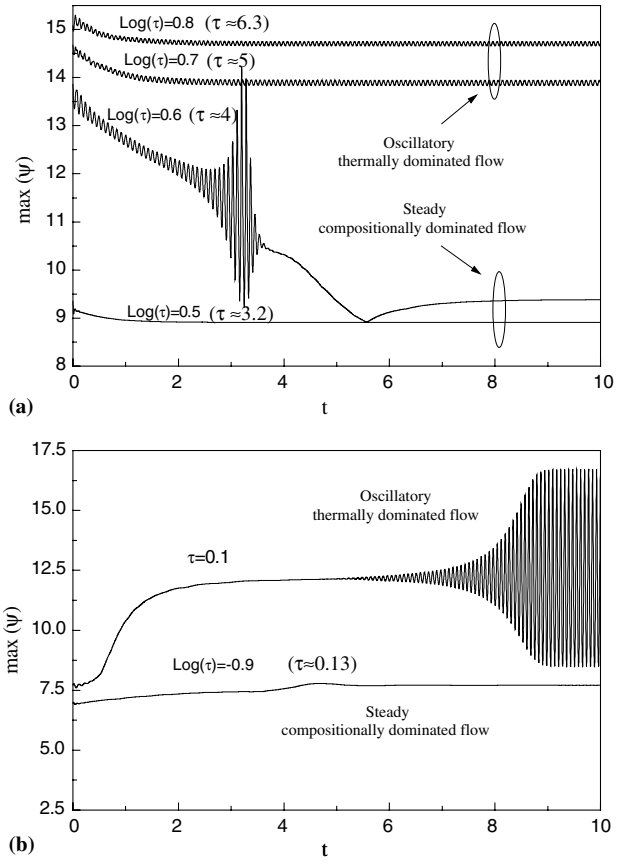

Fig. 11. Effect of the optical thickness on the time behaviour of the maximum stream function for $Pr = 13.6$, $Le = 2$, $Ra = 10^5$, $N = 1$, $\mathrm{Rc} = 1$ and $Ha = 10$ (transitions between steady and oscillatory flows).

the active walls (Fig. 12c). Two significantly developed thermal cells are present near the bottom half of the hot wall and near the top half of the cold wall. This flow structure is similar to that obtained for non-damped flow with $\tau = 1$ and steady compositionally dominated flow as initial condition (Fig. 9). However, when $\log \tau$ changes from 0.6 to 0.7, the oscillatory flow re-emerges via the coalescence of the two thermal cells (Fig. 12d) while the compositional recirculation is partitioned into top left and bottom right compositional cells. At the beginning of this coalescence, the last cited cell is very small. These transitions are accompanied by jumps in the conductive and mass fluxes on the isothermal walls (Fig. 13). However, similar abrupt changes are difficult to read on radiative fluxes which are naturally more sensitive to optical thickness variations. Fig. 13 shows also that heat and mass transfer are more important for oscillatory thermally dominated flow.

Quantitatively, $\overline{Q_r}$ decreases by about 90% when τ changes from 10^{-2} to 10^2. This rate level is identical to that obtained in the non-damped case. The corresponding rates for conductive heat fluxes and Sherwood number are less significant. In another hand, the transitions between steady compositionally dominated flow and oscillatory thermally dominated flow introduce step variation by about 55% for the Sherwood number and 50% for the conductive flux in the optical thin domain. The corresponding values in the optical thick zone are 25% and 15%.

4.1.3. Highly damped flow ($Ha = 40$)

For $Ha = 40$ and independently of the nature of the initial conditions, all computed flows are steady, the magnetic damping is important and the level of the flow intensity is dramatically decreased. In fact $\overline{\max}(\psi)$ decreases by about 95% when Ha changes from 0 to 40. For $\tau = 10^2$ (Fig. 14e), a central thermal cell is in contact with a large compositional cell at the bottom and a weak one near the right top corner. When τ decreases, the bottom compositional cell expands and pushes the thermal cell to the top. Simultaneously, the top compositional cell disappears and a new thermal cell is created at the left bottom corner (Fig. 14c). For $\tau = 0.1$ (Fig. 14b), the flow is compositionally dominated with a large compositional cell working directly between the isothermal walls and two thermal cells at the top right and bottom left corners. When τ decreases again (Fig. 14a), the last cited cell wraps the hot wall.

As expected and due to radiation, temperature distribution is more homogenized than concentration distribution, isotherms are less distorted and there is almost no vertical temperature stratification for all values of the optical thickness.

The effect of the optical thickness on time-averaged heat and mass transfers through isothermal walls are illustrated in Fig. 15. For optically thin media, $\overline{Q_c}$ and $\overline{Sh}$ are approximately equal to the unity. This defines the pure heat conduction and mass diffusion cases which is confirmed by the profile of isotherms and iso-concentrations in Fig. 14a. When τ increases, $\overline{Q_r}$ decreases while $\overline{Q_c}$ manifests a maximum for $\tau \approx 3$ and $\overline{Sh}$ present a stepped variation which is linked to the disappear of the top right compositional cell. Quantitatively, this transition provokes a jump in $\overline{Sh}$ by about 25%, while $\overline{Q_r}$ decreases by about 95% when τ changes from 10^{-2} to 10^2 which is slightly higher than in the non-damped case.

4.2. Effect of scattering albedo

In this section, the effect of the scattering albedo on the flow structure and the magnetic damping of heat and mass transfer is investigated for $Ha = 10$, $\tau = 1$ and $\tau = 10^2$. Solutions for $\omega_0 = 0$ are used as initial conditions and the scattering albedo is affected with values between 0 and 1. Table 2 summarizes the effect of the scattering albedo on time-averaged flow intensity as well as on heat and mass transfers across the isothermal vertical walls for steady compositionally dominated flow ($\tau = 1$) and oscillatory thermally dominated flow ($\tau = 10^2$). For purely scattering media, the temperature distribution is independent of the radiative transfer and as a result, the flow is identical to that obtained for opaque media. Since horizontal walls are perfectly reflecting, the radiative fluxes are identical on the two vertical walls. Also the conservation of the

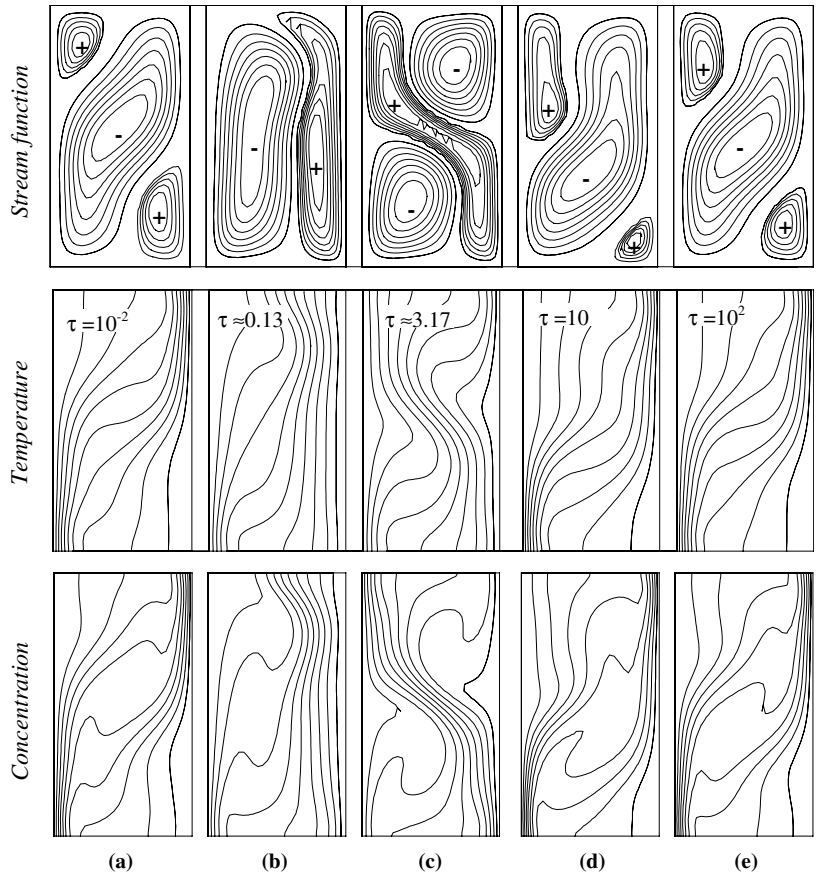

Fig. 12. Effect of the optical thickness on snapshots of oscillatory fields at $t = 0.2$ (a, d and e) and on steady distributions (b and c) for $Pr = 13.6$, $Le = 2$, $Ra = 10^5$, $N = 1$, $\mathrm{Rc} = 1$ and $Ha = 10$. (a) $\max(\psi) = 11.89$, $\min(\psi) = -0.41$ (top cell), -0.67 (bottom cell); (b) $\max(\psi) = 7.71$, $\min(\psi) = -1.53$; (c) $\min(\psi) = -2.26$, $\max(\psi) = 8.27$ (top cell), 8.91 (bottom cell); (d) $\max(\psi) = 15.3$, $\min(\psi) = -1.09$ (top cell), -0.207 (bottom cell); (e) $\max(\psi) = 13.79$, $\min(\psi) = -0.656$ (top cell), -0.517 (bottom cell).

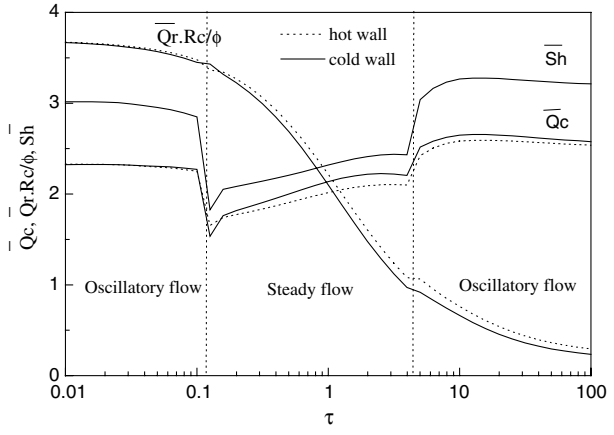

Fig. 13. Effect of the optical thickness on the time-averaged Sherwood number and conductive and radiative fluxes for $Pr = 13.6$, $Le = 2$, $Ra = 10^5$, $N = 1$, $\mathrm{Rc} = 1$ and $Ha = 10$.

conductive fluxes is verified between hot and cold walls since the horizontal walls are adiabatic. Quantitatively and for $\tau = 1$, when ω_0 changes from 0 to 0.8, $\overline{Sh}$ decreases by about 20% and $\overline{Q_c}$ by about 17% on the hot wall and 28% on the cold wall. However, for this variation of ω_0, $\overline{Q_r}$ increases by 0.5% and 10% on the hot and cold walls respectively. Similar behaviours are obtained for the oscillatory flow ($\tau = 10^2$). However, the corresponding conductive heat flux and mass flux rates are less important while the radiative flux rates are more important.

5. Concluding remarks

A numerical model for studying the two-dimensional unsteady hydromagnetic double-diffusive convection in absorbing/emitting and isotropically scattering medium was established using the control volume method for the flow and energy equations and the finite volume method for the radiative transfer equation. The effect of optical properties of the semitransparent fluid on this convection was investigated for different Hartmann numbers. Some concluding remarks can be resumed as follows:

- For all values of optical thickness and Hartmann number, the oscillatory behaviour was not obtained for compositionally dominated flows. This extends to semitransparent media the fact that oscillations appear only in thermally dominated flows.

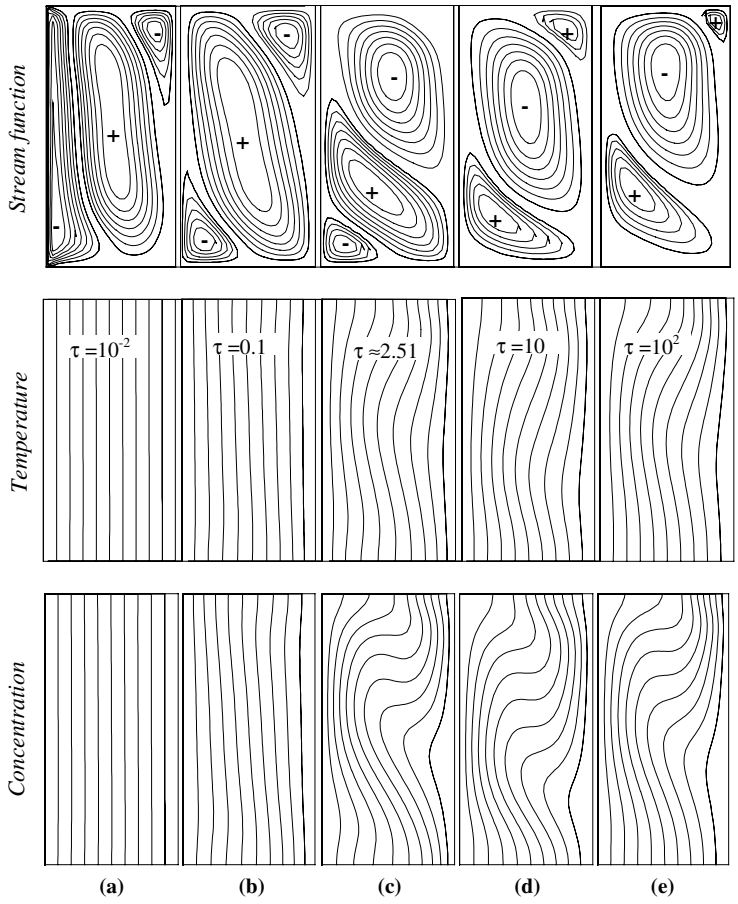

Fig. 14. Effect of the optical thickness on steady stream function, temperature and concentration contours for $Pr = 13.6$, $Le = 2$, $Ra = 10^5$, $N = 1$, $\mathrm{Rc} = 1$ and $Ha = 40$. (a) $\max(\psi) = 1.7510^{-2}$ (left cell), 5.5410^{-3} (right cell); $\min(\psi) = -1.510^{-2}$; (b) $\min(\psi) = -0.234$, $\max(\psi) = 0.102$ (top cell), 7.610^{-2} (bottom cell); (c) $\min(\psi) = -0.683$, $\max(\psi) = 2.237$ (top cell), 0.183 (bottom cell); (d) $\max(\psi) = 2.25$, $\min(\psi) = -0.265$ (top cell), -0.39 (bottom cell); (e) $\max(\psi) = 2.08$, $\min(\psi) = -0.123$ (top cell), -0.232 (bottom cell).

- The stabilizing character of the radiative transfer depends on the Hartmann number affectation. This stabilizing role is clear for optical thickness near unity for moderately damped flow and depends on initial conditions for non-damped flow.

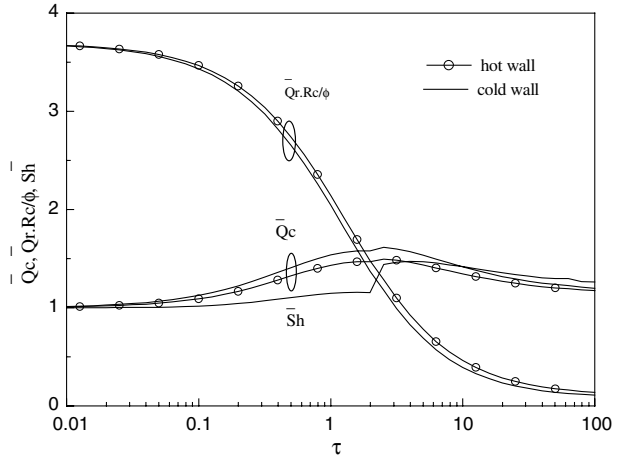

Fig. 15. Effect of the optical thickness on the time-averaged Sherwood number and conductive and radiative fluxes for $Pr = 13.6$, $Le = 2$, $Ra = 10^5$, $N = 1$, $\mathrm{Rc} = 1$ and $Ha = 40$.

- In absence of magnetic damping and depending on initial conditions, dual oscillatory thermal-dominated flow and steady compositional-dominated flow were obtained for optical thickness near unity. The thermally dominated flow is more stable to optical width progres-

Table 2
Effect of the scattering albedo on heat and mass transfers and on flow intensity for $N = 1$, $Le = 2$, $Ra = 10^5$, $Pr = 13.6$ and $Ha = 10$

ω_0	$\overline{\max(\psi)}$	$\overline{Sh}$	$\overline{Q_c}$		$\overline{Q_r}$	
			Hot wall	Cold wall	Hot wall	Cold wall
$\tau = 1$ (*Steady flow*)						
0	6.88	2.319	2.016	2.137	2.217	2.1
0.2	6.83	2.275	1.96	2.071	2.235	2.127
0.4	6.818	2.223	1.897	1.994	2.253	2.159
0.6	6.878	2.156	1.824	1.896	2.271	2.201
0.8	8.009	1.842	1.67	1.529	2.227	2.311
1	11.94	3.019	2.331	2.322	2.319	2.319
$\tau = 10^2$ (*Oscillatory flow*)						
0	13.96	3.213	2.52	2.58	0.295	0.235
0.2	13.96	3.211	2.532	2.571	0.297	0.237
0.4	13.97	3.209	2.524	2.564	0.301	0.241
0.6	13.95	3.207	2.509	2.55	0.308	0.249
0.8	13.9	3.202	2.476	2.518	0.324	0.263
1	11.94	3.02	2.331	2.322	0.209	0.209

sive variations than the compositionally dominated flow. Transitions from steady compositionally dominated convection to unsteady thermally dominated solution were registered for two critical values of the optical thickness. During these transitions a coalescence of the two thermal recirculations was observed simultaneously with the division of the compositional recirculation. No transition from the thermally dominated flow to the compositionally dominated flow was obtained for non-damped flow.

- For moderately damped flow, initial conditions have little effect on the final temporal nature and spatial structure of the flow. Transitions from steady flow to unsteady flow (and reversely) were observed and never oscillatory solutions were obtained for optical thickness near unity.
- For strongly damped flow no oscillatory solution has been observed for all studied values of the optical width and the steady flow intensity is very weak but the flow structure manifests complicated behaviour when the optical thickness changes.
- Transitions from the compositionally dominated to the thermally dominated flows (and reversely) are accompanied by an important increase (decrease) of conductive heat and mass transfers. However radiative heat transfer is almost unaffected by these transitions. These quantitative variations are more important in the optical thin domain for both non-damped and moderately damped flows.
- When the medium scatters radiation, a moderate quantitative influence is observed. However, never qualitative changes are registered except for purely scattering medium where the radiative problem can be treated independently.

References

[1] T. Nishimura, M. Wakamatsu, A.M. Morega, Oscillatory double-diffusive convection in a rectangular enclosure with combined horizontal temperature and concentration gradients, Int. J. Heat Mass Transfer 41 (1998) 1601–1611.

[2] S. Ostrach, Natural convection with combined driving forces, Physico Chem. Hydrodyn. 1 (1980) 233–247.

[3] R. Viskanta, T.L. Bergman, F.P. Incropera, Double-diffusive natural convection, in: Natural Convection: Fundamentals and Applications, Hemisphere, Washington, DC, 1985, pp. 1075–1099.

[4] C. Béghein, F. Haghighat, F. Allard, Numerical study of double-diffusive natural convection in a square cavity, Int. J. Heat Mass Transfer 35 (1992) 833–846.

[5] H. Zhou, A. Zebib, Oscillatory double diffusive convection in crystal growth, J. Cryst. Growth 135 (1994) 587–593.

[6] A.J. Chamkha, H. Al-Naser, Hydromagnetic double-diffuse convection in a rectangular enclosure with opposing temperature and concentration gradients, Int. J. Heat Mass Transfer 45 (2002) 2465–2483.

[7] V.A.F. Costa, Double diffusive natural convection in a square enclosure with heat and mass diffusive walls, Int. J. Heat Mass Transfer 40 (1997) 4061–4071.

[8] V.A.F. Costa, Double-diffusive natural convection in parallelogrammic enclosures, Int. J. Heat Mass Transfer 47 (2004) 2913–2926.

[9] E. Papanicalaou, V. Belessiotis, Double-diffusive natural convection in an asymmetric trapezoidal enclosure: unsteady behavior in the laminar and the turbulent-flow regime, Int. J. Heat Mass Transfer 48 (2005) 191–209.

[10] K. Kamakura, H. Ozoe, Experimental and numerical analyses of double diffusive natural convection heated and cooled from opposing vertical walls with an initial condition of a vertically linear concentration gradient, Int. J. Heat Mass Transfer 36 (1993) 2125–2134.

[11] J.P. Garandet, T. Aboussiere, R. Moreau, Buoyancy driven convection in a rectangular enclosure with a transverse magnetic field, Int. J. Heat Mass Transfer 35 (1992) 741–748.

[12] R. Mößner, U. Müller, A numerical investigation of three-dimensional magnetoconvection in rectangular cavities, Int. J. Heat Mass Transfer 42 (1999) 1111–1121.

[13] S. Alexandrova, S. Molokov, Three-dimensional buoyant convection in a rectangular cavity with differentially heated walls in a strong magnetic field, Fluid Dyn. Res. 35 (2004) 37–66.

[14] S. Kenjereš, K. Hanjalić, Numerical simulation of magnetic control of heat transfer in thermal convection, Int. J. Heat Fluid Flow 25 (2004) 559–568.

[15] T. Tsukada, K. Kakinoki, M. Hozawa, Effect of internal radiation within crystal and melt on Czochralski crystal growth of oxide, Int. J. Heat Mass Transfer 38 (1995) 2707–2714.

[16] M. Kobayachi, T. Tsukada, M. Hozawa, Effect of internal radiative heat transfer on the convection in CZ oxide melt, J. Cryst. Growth 180 (1997) 157–166.

[17] M. Kobayachi, T. Tsukada, M. Hozawa, Effect of internal radiative heat transfer on transition of flow modes in CZ oxide melt, J. Cryst. Growth 208 (2000) 459–465.

[18] M. Kobayachi, T. Hagino, T. Tsukada, M. Hozawa, Effect of internal radiative heat transfer on interface inversion in Czochralski crystal growth of oxides, J. Cryst. Growth 235 (2002) 258–270.

[19] C.J. Jing, A. Hayachi, M. Kobayachi, T. Tsukada, M. Hozawa, N. Imaishi, K. Shimamura, N. Ichinose, Effect of internal radiative heat transfer on spoke pattern on oxide melt surface in Czochralski crystal growth, J. Cryst. Growth 259 (2003) 367–373.

[20] C.W. Lan, C.Y. Tu, Y.F. Lee, Effects of internal radiation on heat flow and facet formation in Bridgman growth of YAG crystals, Int. J. Heat Mass Transfer 46 (2003) 1629–1640.

[21] S. Brandon, J.J. Derby, Internal radiative transport in the vertical Bridgman growth of semitransparent crystals, J. Cryst. Growth 110 (1991) 481–500.

[22] G. Müller, J. Friedrich, Challenges in modeling of bulk crystal growth, J. Cryst. Growth 266 (2004) 1–19.

[23] C.J. Jing, N. Imaishi, T. Sato, Y. Miyazawa, Three-dimensional numerical simulation of rotating spoke pattern in an oxide melt under a magnetic field, Int. J. Heat Mass Transfer 43 (2000) 4347–4359.

[24] M.V. Farrell, N. Ma, Macrosegregation during alloyed semiconductor crystal growth in strong axial and transverse magnetic fields, Int. J. Heat Mass Transfer 47 (2004) 3047–3055.

[25] R. Siegel, J.R. Howell, Thermal radiation heat transfer, third ed., Hemisphere Publishing, New York, 1992.

[26] J.C. Chai, H.S. Lee, S.V. Patankar, Finite volume method for radiative heat transfer, J. Thermophys. Heat Transfer 8 (1994) 419–425.

[27] M.N. Borjini, H. Farhat, M.S. Radhouani, Analysis of radiative heat transfer in a partitioned idealized furnace, Numer. Heat Transfer, Part A 44 (2003) 199–218.

[28] S.V. Patankar, Numerical Heat Transfer and Fluid Flow, McGraw Hill, New York, 1980.

[29] A. Bejan, Convection Heat Transfer, John Wiley and Sons, New York, 1984.

[30] M.N. Borjini, C. Mbow, M. Daguenet, Numerical analysis of the effect of radiation on laminar steady natural convection in a two-dimensional participating medium between two horizontal confocal elliptical cylinders, Numer. Heat Transfer, Part A 35 (1999) 467–494.

[31] M.N. Borjini, C. Mbow, M. Daguenet, Numerical analysis of combined radiation and unsteady natural convection within a horizontal annular space, Int. J. Numer. Methods Heat Fluid Flow 9 (1999) 742–764.
[32] S. Uda, W.A. Tiller, The dissociation and ionization of $LiNbO_3$ melts, J. Cryst. Growth 121 (1992) 155–190.
[33] I. Sezai, A.A. Mohamad, Double diffusive convection in a cubic enclosure with opposing temperature and concentration gradients, Phys. Fluids 12 (9) (2000) 2210–2223.
[34] M. Mamou, P. Vasseur, E. Bilgen, Multiple solutions for double-diffusive convection in a vertical porous enclosure, Int. J. Heat Mass Transfer 38 (1995) 1787–1798.